

# Sea Surface Temperature Modification of Low-Level Winds

Dudley B. Chelton

*College of Oceanic and Atmospheric Sciences, 104 Oceanography Administration Building,  
Oregon State University, Corvallis, OR 97331-5503  
Email: [chelton@coas.oregonstate.edu](mailto:chelton@coas.oregonstate.edu)*

## 1. Introduction

Numerous in situ observational studies have called attention to the existence of strong sea surface temperature (SST) effects on low-level winds (see the historical review in Section 2 of O'Neill et al., 2003). The availability of the multi-year, global record of surface wind stress observations with high spatial resolution and dense coverage from the QuikSCAT radar scatterometer has revealed the remarkable intensity and apparent ubiquitous existence of this air-sea interaction in regions of strong SST gradients throughout the world ocean. The coupling between SST and low-level winds is especially clear in the eastern tropical Pacific (Xie et al., 1998; Chelton et al., 2001; Hashizume et al., 2001) and over the Southern Ocean (O'Neill et al., 2003), where meanders of the SST fronts provide unambiguous and detailed evidence of the nature of this air-sea interaction. The objective of this study is to investigate whether SST influence on low-level winds can be detected in the surface wind stress fields produced by the ECMWF model.

The various datasets analyzed in this study are briefly summarized in Section 2. The effects of SST on surface wind stress in the eastern tropical Pacific and the Southern Ocean are summarized in Sections 3 and 4, respectively. In each of these sections, the coupling is first described from QuikSCAT observations and then from ECMWF model forecast surface wind stress fields. The conclusions are summarized in Section 5.

## 2. Data

The primary datasets for this analysis are the surface wind stresses from QuikSCAT observations and from the ECMWF model for the 12-month time period August 1999 through July 2000, corresponding to the first 12 months of the QuikSCAT mission. These datasets are briefly summarized here.

The QuikSCAT scatterometer infers surface wind stress magnitude and direction with a resolution of 25 km from measurements of microwave radar backscatter received from a given location on the sea surface at multiple antenna look angles. Scatterometer wind stress retrievals are calibrated to the neutral-stability wind at a height of 10 m. Wind stress is computed from the 10-m neutral stability wind by the bulk formulation with a neutral stability drag coefficient (e.g., Large and Pond, 1981). For the present analysis, the QuikSCAT wind stress measurements were smoothed and interpolated onto a  $0.5^\circ$  grid at 1-day intervals using a loess smoother (Schlax et al., 2001) with filter cutoff wavelengths of  $4^\circ$  of longitude by  $2^\circ$  of latitude and a filter cutoff period of 8 days. These filter cutoffs are similar to the filter transfer function of  $2.4^\circ$  by  $1.2^\circ$  by 4.8-day block averages, except that the filter side lobes are much smaller for the loess smoother (see Fig. 1 of Chelton and Schlax, 2003).

The ECMWF wind stress fields used here are the 6-hour forecast fields obtained directly from the ECMWF model, obviating the need for use of the bulk formulation. While the T319 spherical harmonic model used by ECMWF during the time period considered here had a grid resolution of  $0.565^\circ$ , these wind stress fields were archived on a  $1.125^\circ$  grid at 6-hour intervals. Furthermore, the stresses were available as “accumulated stress” over each 6-hour interval, i.e., the integral of the wind stress. For the analyses presented here, these

accumulated stresses were converted to stress by dividing by the 6-hour time interval. The time tag of each 6-hourly accumulated wind stress field should probably be adjusted backward 3 hours from the forecast time to account for this averaging period, but this was not done for the analyses presented here. The 6-hourly ECMWF wind stress fields were averaged daily and interpolated onto the same  $0.5^\circ$  by 1-day grid as the QuikSCAT wind stress fields. No additional smoothing was applied to the ECMWF stress fields. In particular, the  $4^\circ$  by  $2^\circ$  by 8-day smoothing that was applied to the QuikSCAT observations was not applied to the ECMWF wind stress fields.

The wind stress curl and divergence fields from which the SST effects on low-level winds are diagnosed in Sections 3 and 4 were computed from the  $0.5^\circ$ -gridded QuikSCAT and ECMWF wind stress fields by centered first differences.

To assess the influence of SST on the surface wind stress, different SST datasets are used in different parts of this study. The effects of SST on the observed wind stress fields obtained from QuikSCAT data should be determined from observed SST. For the eastern tropical Pacific analyses of QuikSCAT data in Section 3, observed SST was obtained from the Tropical Rainfall Measuring Mission (TRMM) Microwave Imager (TMI) (Wentz et al., 2000). The TMI observations were smoothed with the same loess smoothing parameters applied to the QuikSCAT wind stress observations and were gridded onto the same  $0.5^\circ$  by 1-day grid.

The orbit inclination of the TRMM satellite limits the TMI data to latitudes lower than  $38^\circ$ . The availability of microwave observations of SST from the Advanced Microwave Scanning Radiometer (AMSR) on the EOS Aqua satellite beginning in July 2002 and on the ADEOS-II satellite launched in December 2002 will allow higher-latitude comparisons of QuikSCAT winds with high-resolution SST fields in the near future. However, since all-weather microwave observations of SST are not available at latitudes higher than  $38^\circ$  for the time period considered here, it was necessary to use the “Reynolds SST fields” for the Southern Ocean analyses of QuikSCAT data in Section 4. As described by Reynolds and Smith (1994), these SST fields were computed as weekly averages on a  $1^\circ$  grid from a blending of in situ and satellite infrared measurements of SST. For the present study, these weekly average SST analyses were interpolated onto the same  $0.5^\circ$  by 1-day grid as the QuikSCAT wind stress and TMI SST fields.

For assessment of the ECMWF representation of SST-induced perturbations of the surface wind stress fields, it is most appropriate to compare the ECMWF stresses with the SST fields that are used as the surface boundary condition in the ECMWF model. For the August 1999 through July 2000 time period under consideration here, these consisted of Reynolds analyses of weekly average SST updated at daily intervals. These daily Reynolds analyses of weekly average SST are not as readily available as the weekly analyses of weekly average SST. The weekly analyses are therefore utilized in this study.

Because of the details of the nonlinear analysis procedure (Reynolds and Smith, 1994), the weekly average SST fields produced at daily and weekly intervals for the same 7-day time period are not identical. For present purposes, however, the differences are minor with one important exception: the time tags on the daily analyses of weekly average SST used as the surface boundary condition in the ECMWF model are 3.5 days later than the midpoint of each 7-day average SST field. Thus, for example, the time tag on the daily analysis of average SST over the period 1–7 January is 0000 UTC on 8 January (R. Reynolds, 2003, personal communication). For the same 7-day averaging period, the time tag for the weekly Reynolds analyses utilized in this study would be 1200 UTC on 4 January, i.e., the midpoint of the 7-day averaging period. It is shown in Section 3 that the 3.5-day lag in the time tag for the daily analysis apparently has a measurable impact on the accuracy of the ECMWF wind fields, at least in the eastern tropical Pacific.

QuikSCAT Wind Stress and TMI SST, 4 September 1999

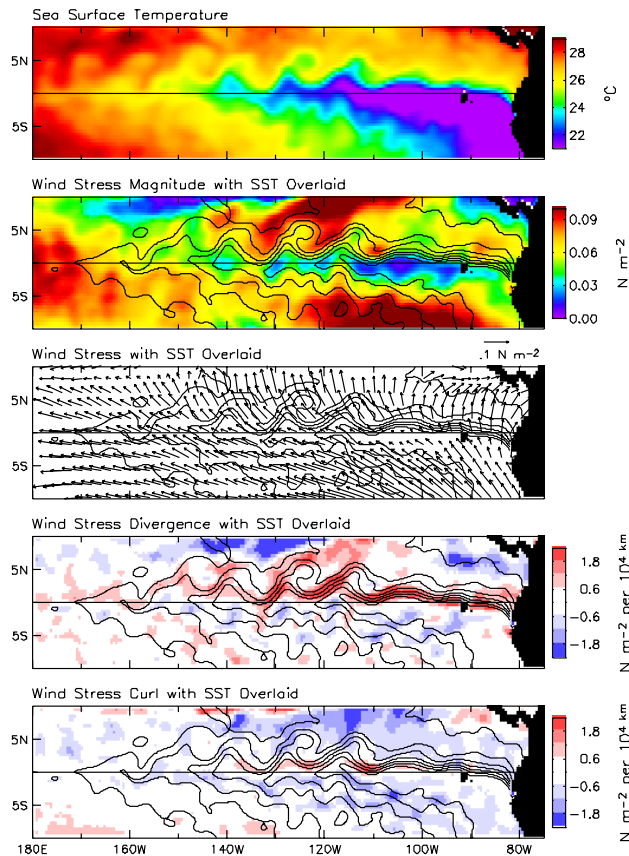


Figure 1 Maps for 4 September 1999 derived from QuikSCAT observations of wind stress and TMI observations of SST with spatial and temporal smoothing as described in the text. The SST in the top panel is overlaid with a contour interval of 1°C in the bottom four panels.

Time–Longitude Plots Along 1°N, QuikSCAT Wind Stress and TMI SST

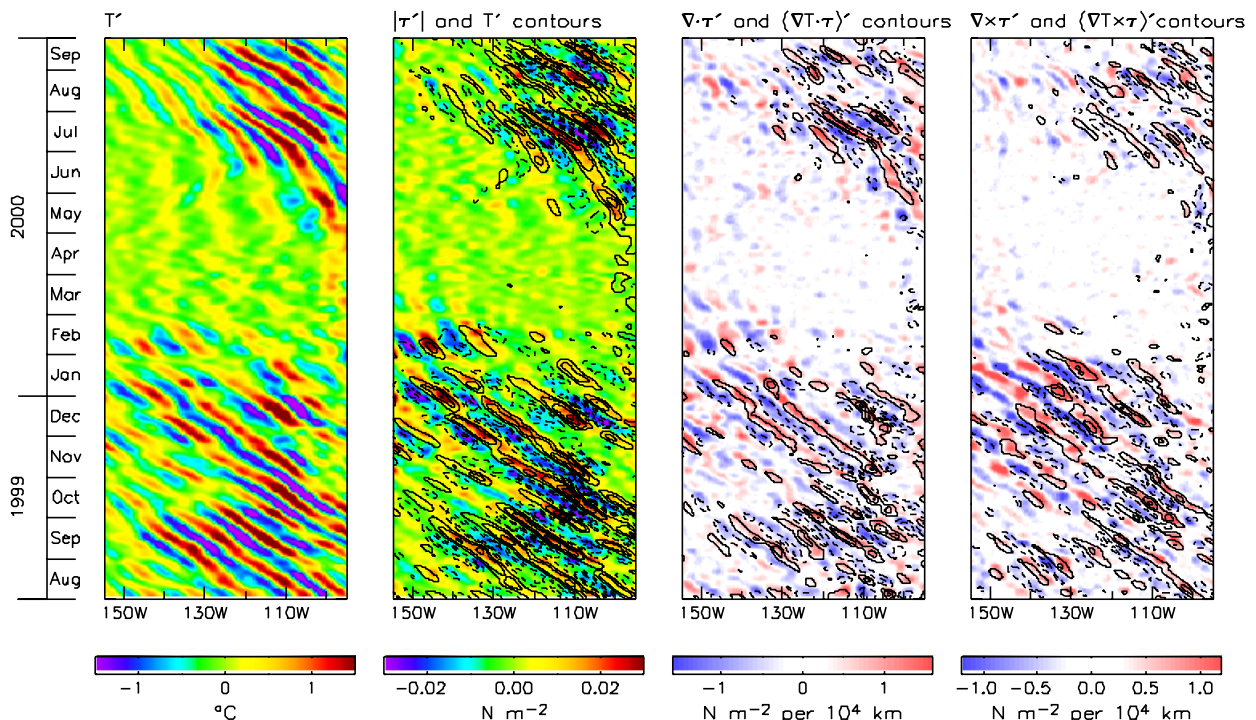


Figure 2 Time-longitude plots of QuikSCAT observations of wind stress and TMI observations of SST along 1°N showing westward propagation of SST, wind stress magnitude, wind stress divergence and wind stress curl (left to right) after zonally high-pass filtering to remove wavelengths longer than 20° of longitude. SST from the first panel is overlaid with a contour interval of 0.5°C in the second panel. The contours in the right two panels are the downwind and crosswind SST gradients, respectively, with contour intervals of 0.4°C per 100 km. The zero contours have been omitted from the three right panels for clarity.

### 3. Eastern Tropical Pacific

SST modification of low-level winds in the eastern tropical Pacific is clearly evident in the QuikSCAT and TMI data (Figs. 1 and 2). In the example map from 4 September 1999 in the upper panel of Fig. 1, the SST fronts that bracket the equatorial cold tongue are evident as cuspy patterns along the north and south sides of the cold tongue. These cuspy patterns are the signatures of transequatorial tropical instability waves (TIWs) that propagate westward on both sides of the equator at about 0.5 m/s with periods of about a month and wavelengths of about 1200 km (Chelton et al., 2000). From the second panel of Fig. 1, it is evident that the wind stress is weak over cold water and strong over warm water. The cuspy patterns in the SST fields are faithfully reproduced in the wind stress fields. The SST and wind stress perturbations are seen to propagate synchronously westward in the left two panels of Fig. 2.

The coupling between SST and wind stress that is evident in Figs. 1 and 2 was first noted from climatological data by Wallace et al. (1989). The boundary layer dynamics responsible for this coupling are not yet understood in detail, but they are evidently related to SST modification of the stability of the atmospheric boundary layer. Wallace et al. (1989) hypothesized that stabilization of the boundary layer over cold water decouples the surface winds from the winds aloft, resulting in light winds at the sea surface. Increased vertical turbulent mixing over warm water increases the winds at the sea surface through downward mixing of momentum from aloft. As first noted by Hayes et al. (1989), the existence of TIWs provides a stringent test of this hypothesized SST-induced modification of atmospheric boundary layer stability. The close agreement between the patterns and westward propagation of SST and wind stress anomalies in Figs. 1 and 2 implies that the boundary layer response to SST is very rapid.

Geographical variations of the wind stress field in the vicinity of strong SST gradients result in wind stress divergence and curl that are directly related to the SST patterns (Chelton et al., 2001). Accelerations of surface winds blowing across SST fronts result in a divergence of the wind stress. Likewise, lateral variations of surface winds blowing parallel to SST fronts result in a curl of the wind stress. These associations of the wind stress divergence and curl with the downwind and crosswind components of SST gradient are visually evident in the lower two panels of Fig. 1 and are shown quantitatively in the left panels of Fig. 3 by the cosine and sine dependencies of divergence and curl on the angle between the SST gradient vector and the wind direction.

By the above arguments, the wind stress divergence and curl should vary linearly with the downwind and crosswind components of the SST gradient, respectively. This is indeed the case, as shown by the red lines in the right panels of Fig. 3, which represent least squares line fits to binned averages of divergence and curl anomalies as functions of the perturbations of the SST gradient components on the north side of the equatorial cold tongue. The perturbation downwind and crosswind components of TMI SST gradients overlaid as contours on the right two panels of Fig. 2 are seen to coincide with the perturbation QuikSCAT wind stress divergence and curl, respectively. The wind stress divergence and curl anomalies propagate synchronously westward with the SST gradient component anomalies.

SST Perturbations of Wind Stress Curl and Divergence, August 1999–January 2000

3°N to 1°S, QuikSCAT vs. TMI, ECMWF vs. Reynolds

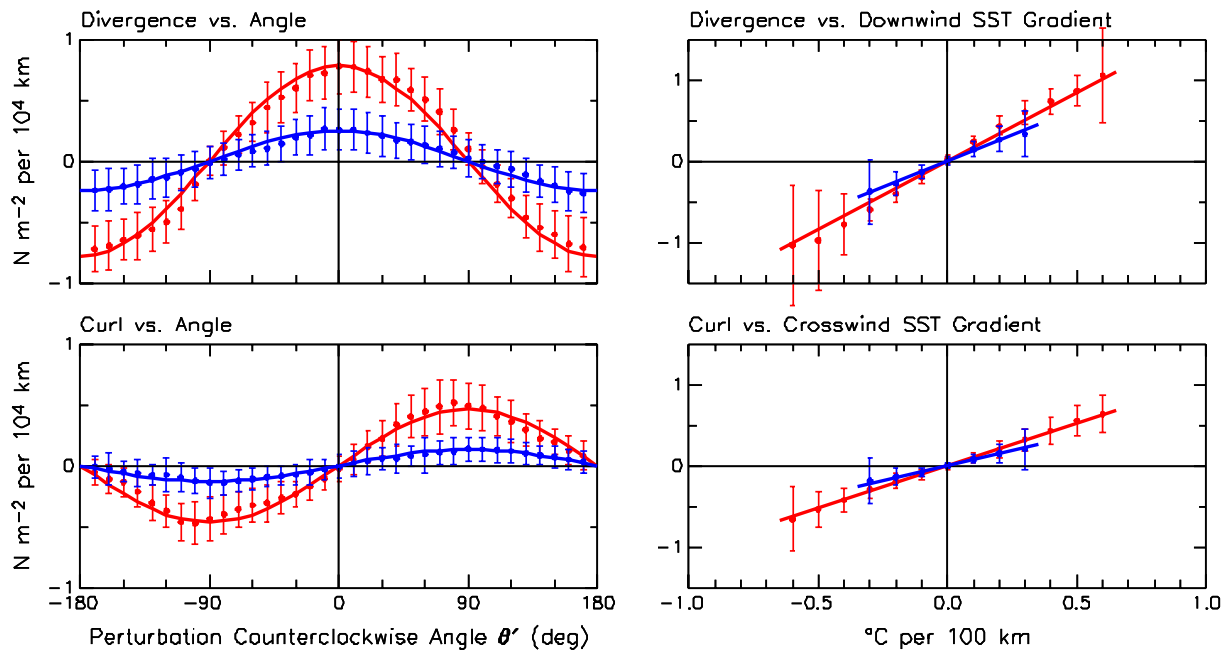


Figure 3 Left: Binned scatterplots of the angular dependencies of zonally high-pass filtered wind stress divergence (top) and curl (bottom) on the angle between the SST gradient vector and the wind direction in the region 150°–100°W and 1°S to 3°N. Right: Binned scatterplots of the relationships between zonally high-pass filtered wind stress divergence and the downwind gradient of SST (top) and between the zonally high-pass filtered wind stress curl and the crosswind gradient of SST (bottom). The error bars in all plots represent the standard deviations of the scatter within each bin. The red lines are the results obtained from the QuikSCAT and TMI observations and the blue lines are the results obtained from the ECMWF model wind stresses and Reynolds SST analyses.

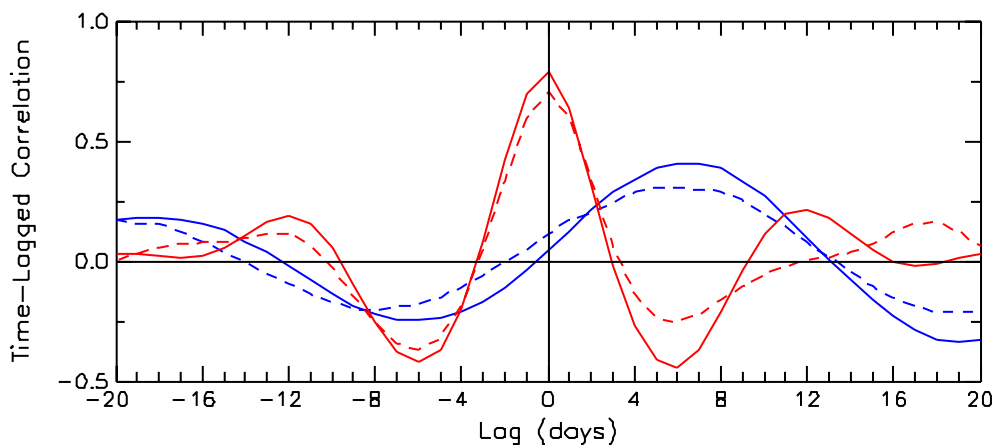


Figure 4 Lagged cross correlations between the wind stress divergence and the downwind gradient of SST (solid lines) and between the wind stress curl and the crosswind gradient of SST (dashed lines). Positive lags correspond to SST leading the wind stress. The red lines are the results obtained from the QuikSCAT and TMI observations and the blue lines are the results obtained from the ECMWF model wind stresses and Reynolds SST analyses.

Analysis of the relationship between Reynolds SST and the ECMWF wind stress divergence and curl in the eastern tropical Pacific revealed a systematic lag, with wind stress lagging SST by 6–7 days (see the blue lines in Fig. 4). This lag has been independently confirmed from comparisons between the daily Reynolds

analyses of weekly averaged SST that were used as the surface boundary condition in the ECMWF model and observations from moorings at 2.8°S, 124.7°W and 10.0°N, 125.4°W. For the 16-month period May 1997 through September 1998, the maximum correlation at both locations was at a lag of 6.75 days (A. Beljaars, 2003, personal communication). As shown by the red lines in Fig. 4, there is no lag between the QuikSCAT wind stress fields and the TMI SST fields. Moreover, the maximum correlation between TMI and Reynolds SST also occurs at zero lag (not shown here). The lag between the ECMWF wind stress and the Reynolds SST is therefore not due to timing errors in the weekly Reynolds analyses of weekly averaged SST utilized here.

The existence of the 6–7 day lag in the ECMWF winds is undoubtedly related to the fact that it is not possible to obtain real-time SST for the surface boundary condition in the ECMWF model. As discussed in Section 2, the SST boundary condition during the August 1999 through July 2000 time period under consideration here consisted of daily updates of Reynolds weekly averaged SST with time tags at the end of each weekly averaging period. The SST boundary condition for any particular analysis time therefore consisted of the weekly average SST for the previous week. In contrast, the time tags on the weekly Reynolds analyses of weekly average SST utilized here were at the center of each weekly average. The offsets between the time tags on the daily and weekly Reynolds analyses for the same weekly average SST account for 3.5 days of the observed 6–7 day lag in Fig. 4. Another 0.5-day lag can be accounted for by the fact that each 1-week average SST field was used as the surface boundary condition for 24 hours until the next daily update of the 1-week average Reynolds analysis became available. An explanation for the remaining 2–3 day lag between ECMWF wind stress and weekly Reynolds SST analyses proved to be beyond the scope of this study.

To adjust for the erroneous time lag between the daily Reynolds analyses of weekly averaged SST and the ECMWF wind stress, the ECMWF wind stress fields analyzed here were shifted by 7 days. Maps of SST from the Reynolds analyses and the 7-day shifted wind stress fields (magnitude, vectors, divergence and curl) are shown in Fig. 5 for the same 4 September 1999 time for which the TMI SST and QuikSCAT wind stress fields are shown in Fig. 1. While the major features (e.g., the four well-defined cusps along the northern SST front at about 102°W, 112°W, 125°W and 138°W) are recognizable in the Reynolds SST fields, they are smaller in amplitude and considerably smoother spatially than the same features in the TMI SST fields in the upper panel of Fig. 1. The ECMWF wind stress field in the second and third panels of Fig. 5 is not nearly as closely related to the wind stress observed by QuikSCAT (compare with the second and third panels of Fig. 1), but it does at least retain the salient feature of low wind stress in the vicinity of the cold tongue. There is also some resemblance between the ECMWF and QuikSCAT wind stress divergence fields along the north side of the cold tongue. The ECMWF wind stress curl perturbations are too weak to see any similarity with the QuikSCAT wind stress curl field.

The discrepancies between the QuikSCAT and ECMWF wind stress fields are not necessarily bothersome from the perspective of the performance of the ECMWF model. It is conceivable that the boundary layer processes that are responsible for the divergence and curl anomalies are adequately parameterized in the ECMWF model and that the differences between the observed and modeled wind stress divergence and curl perturbations are at least partly attributable to inadequacies in the Reynolds SST fields that are used as the surface boundary condition in the ECMWF model. This appears to be confirmed by the blue lines in Fig. 3, which represent least squares line fits to the binned averages of wind stress divergence and curl as functions of downwind and crosswind SST gradients, respectively. Although the SST perturbations are much weaker in the Reynolds SST analyses, it is evident that the wind stress divergence and curl in the ECMWF analyses are linearly related to the downwind and crosswind SST gradients with coupling coefficients (i.e., the slopes of the line fits) that are only slightly weaker than the coupling coefficients between the QuikSCAT derivative wind stress fields and the TMI SST gradient component fields (the red lines in Fig. 3).

ECMWF Wind Stress and Reynolds SST, 4 September 1999

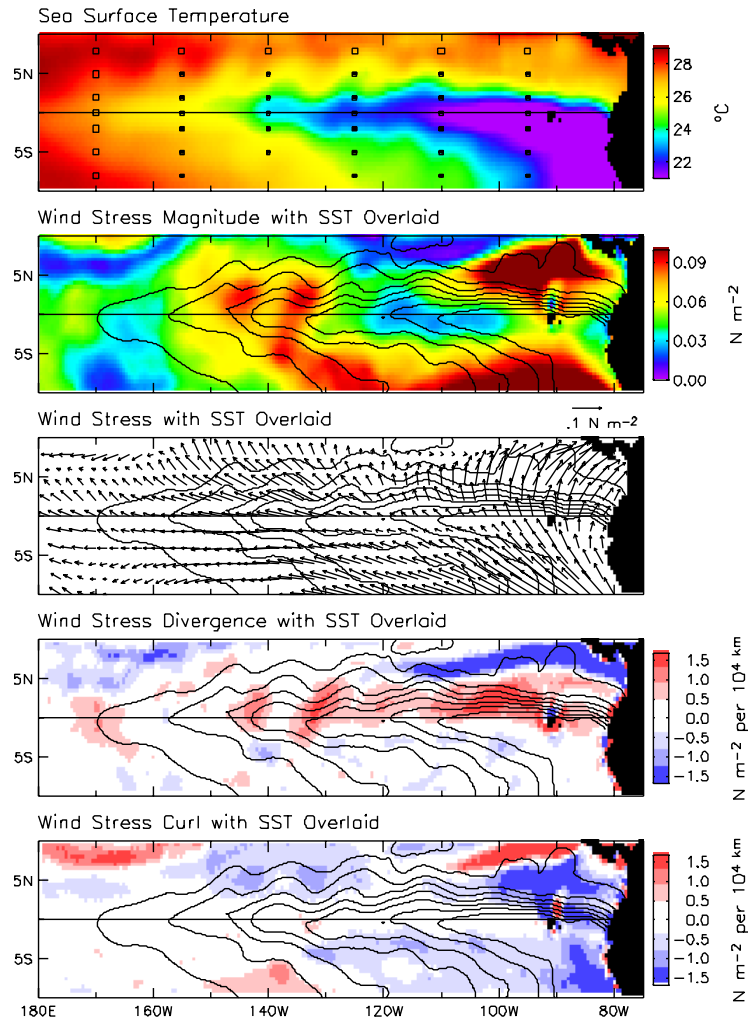


Figure 5 The same as Fig. 1, except derived from the ECMWF model wind stresses and Reynolds SST analyses. Note that the color bars on the bottom two panels are different from the color bars on the bottom two panels of Fig. 1.

The smaller amplitude SST anomalies in the Reynolds analyses thus account for most of the smaller amplitude divergence and curl anomalies in the ECMWF wind stress fields. Model resolution may also be a limitation in the ECMWF wind stress analyses, but this is difficult to assess because of the resolution limitation of the Reynolds SST analyses.

The collocations of the perturbation downwind and crosswind Reynolds SST gradients with the 7-day shifted ECMWF wind stress divergence and curl perturbations are apparent from the contours overlaid on the right panels of Fig. 6. As in the QuikSCAT and TMI observations in Fig. 2, the perturbations of the 7-day shifted ECMWF derivative wind stress fields propagate synchronously westward with the perturbations in the Reynolds SST gradient component fields.

## Time–Longitude Plots Along 1°N, ECMWF Wind Stress and Reynolds SST

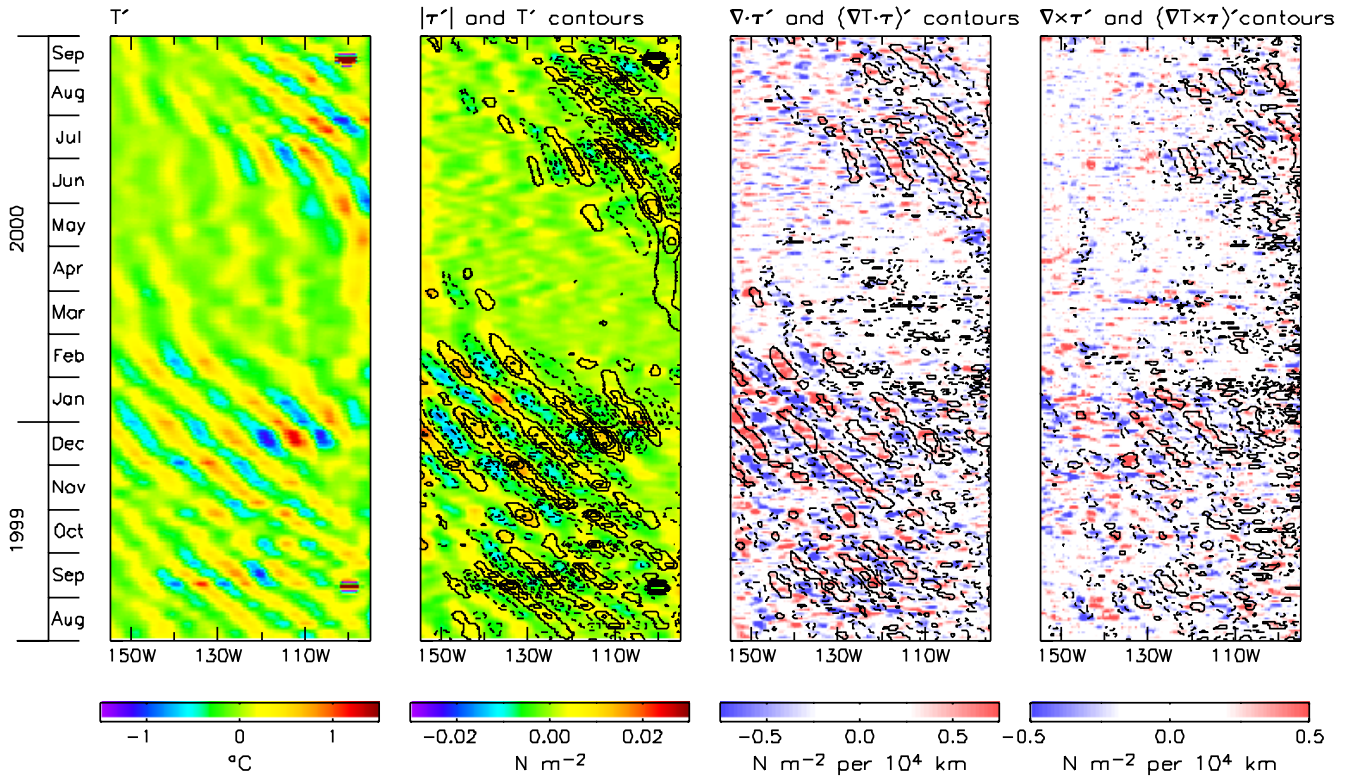


Figure 6 The same as Fig. 2, except from the ECMWF model wind stresses and Reynolds SST analyses along 1°N. The contour intervals are 0.25°C in the second panel and 0.25°C per 100 km in the right two panels. Note that the color bars on the right two panels are different from the color bars on the right two panels of Fig. 2.

Aside from the issue of the 6–7 day lag and a possible model resolution limitation, we conclude that the coupling between SST and wind stress was well represented in the ECMWF analyses in the eastern tropical Pacific during the August 1999 through July 2000 time period under consideration here. With higher model resolution and more accurate SST fields for the surface boundary condition in the ECMWF model, it can be anticipated that the magnitudes of the ECMWF wind stress divergence and curl perturbations would increase and more accurately represent the observed wind stress patterns.

It is noteworthy that a lag between the SST boundary condition and ECMWF analyses of low-level winds is also evident in ECMWF wind fields examined for the more recent August 2001 through January 2003 time period, but with a shorter time lag of 1 day (not shown here). Beginning on 9 May 2001, the daily Reynolds analyses of weekly averaged SST were replaced with the Real-Time Global (RTG) SST analyses produced by the National Centers for Environmental Prediction (NCEP). These RTG SST fields are available as 24-hour averages at 1-day intervals with a time tag at the beginning of the day of each daily analysis period (B. Katz, 2003, personal communication). For each analysis, the time window is extended back to 1015 UTC on the previous day to assimilate any late-arriving observations that were missed in the previous daily analysis; observations from 1015 UTC to 2400 UTC of the previous day are not reused if they arrived in time for the previous daily analysis. For the daily RTG analysis of SST for the 36-hour period from 1015 UTC on 1 January to 2215 UTC on 2 January, for example, the most representative time for the average SST field is probably 1200 UTC on 2 January. However, the NCEP time tag for this analysis is 12 hours earlier, i.e., at 0000 UTC on 2 January.

From an examination of a few recent ECMWF analysis fields (H. Hersbach and ECMWF colleagues, 2003, personal communication), the NCEP time tag on each daily RTG SST field is advanced 36 hours for

implementation as the SST boundary condition in the ECMWF model. The ECMWF-adjusted time tag for the above example of the RTG SST analysis for 1015 UTC on 1 January to 2215 UTC on 2 January would be 1200 UTC on 3 January. Each 1-day average SST field is used as the surface boundary condition for 24 hours until the next 1-day average RTG SST analysis becomes available.

The lag of maximum correlation between the non time-shifted RTG SST fields and ECMWF wind stress (not shown here) is 1 day in the August 2001 through January 2003 ECMWF fields. Assuming that a 36-hour time advance was applied throughout this time period, the 1-day lag is commensurate with the shorter 1-day averaging period of each SST field compared with the 1-week averages used by ECMWF prior to 9 May 2001. Thus, in contrast to the ECMWF stress fields from the earlier August 1999–July 2000 time period considered in Figs. 4–6, it appears that the observed 1-day lag between the more recent ECMWF wind fields and the RTG SST fields is completely accounted for.

Unless SST fields can be made available in real time for the surface boundary condition in the ECMWF model, some lag between the model winds and SST seems inevitable. Observations from the two AMSR instruments that are presently in operation on the EOS Aqua satellite and the ADEOS-II satellite could, at least in principle, be used to construct global real-time SST fields. Presently, however, the AMSR data are not available in real time.

For the purposes of the present study, the sensitivity of the ECMWF wind fields to the detailed specification of the SST boundary condition (i.e., weekly versus daily averages) is a clear indication of the importance of SST to low-level winds in the ECMWF model. This can be taken as evidence that the air-sea interaction process of interest in this study exists within the ECMWF model.

#### **4. Southern Ocean**

Outside of the tropics, the coupling between SST and low-level winds is more difficult to distinguish because it is often overwhelmed by the much more energetic variability at short time scales associated with synoptic weather variability. The effects of SST on wind stress become clear, however, when the SST and wind stress fields are averaged over periods of a few months or more (O'Neill et al., 2003). For the analysis presented here, the QuikSCAT and ECMWF wind stress fields were averaged over the 12-month period August 1999 through July 2000. The effects of the 6–7 day lag between the Reynolds SST analyses and the ECMWF winds discussed in Section 3 are negligible in these 12-month averages.

The global 12-month average wind stress divergence field computed from QuikSCAT observations is shown in the upper left panel of Fig. 7. The strong bands of negative divergence between about 5°N and 10°N in both the Pacific and Atlantic are the Intertropical Convergence Zones, which are not related to the air-sea interaction signals of interest here. The zonal band of positive divergence just north of the equator in the eastern and central Pacific is the time-averaged effect of the TIW-induced SST perturbations of the wind stress divergence field discussed in Section 3. A weaker rendition of this feature exists in the equatorial Atlantic. Outside of these equatorial regions, the most interesting features in the divergence field are the patchy patterns of positive and negative divergence in the regions of strong SST fronts associated with the major ocean currents in the world ocean, most notably the Antarctic Circumpolar Current, the Gulf Stream and the Kuroshio Extension. As shown below, these features represent perturbations of the winds blowing across persistent meandering isotherms in the 12-month average SST field.

The global 12-month average wind stress curl field from QuikSCAT observations is shown in the upper left panel of Fig. 8. Short-scale patchiness is evident in the same regions of wind stress divergence patchiness, although this is more difficult to identify because of the background large-scale wind stress curl patterns associated with the tradewinds and the midlatitude westerly wind belts. When the 12-month average wind stress curl field is spatially high-pass filtered with a loess smoother to remove features with scales larger than

$30^\circ$  of longitude by  $10^\circ$  of latitude (analogous to removing  $18^\circ$  by  $6^\circ$  spatial averages), the patchiness in the short-scale wind stress curl field (the upper right panel of Fig. 8) is seen to be similar to that in the wind stress divergence field. The results from the same filtering applied to the 12-month average wind stress divergence are shown in the upper right panel of Fig. 7. The differences between the unfiltered and the spatially high-pass filtered divergence fields are much smaller than in the case of the wind stress curl fields, reflecting the tendency for winds to be quasigeostrophic, i.e., nondivergent.

As short-scale variability in the wind stress divergence and curl fields is most extensive and well defined in the Southern Ocean region ( $30^\circ\text{S}$  to  $60^\circ\text{S}$ ), the present study focuses on this region to investigate the hypothesis that this midlatitude patchiness in the QuikSCAT wind stress observations is attributable to the same SST modification of low-level winds that was observed in the eastern tropical Pacific (Section 3). Because satellite microwave observations of SST were not available south of  $38^\circ\text{S}$  during the August 1999 through July 2000 time period under consideration here, the spatially high-pass filtered QuikSCAT wind stress divergence and curl fields were compared with the downwind and crosswind SST gradient fields computed from the Reynolds SST analyses averaged over this 12-month period. The downwind and crosswind gradients of the 12-month average Reynolds SST field were spatially high-pass filtered in the same manner as the wind stress divergence and curl fields.

1-Year Average Wind Stress Divergence  
 August 1999 – July 2000

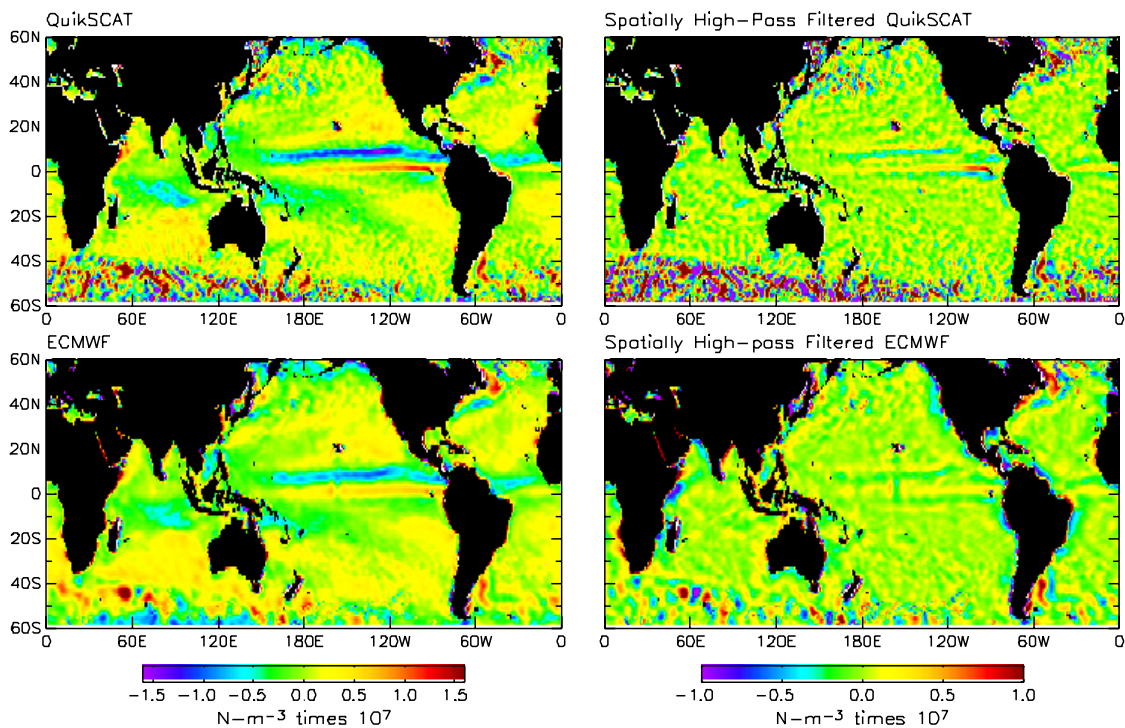


*Figure 7 Average maps of the wind stress divergence over the 12-month period August 1999 through July 2000 derived from QuikSCAT observations (top) and the ECMWF model (bottom). The right panels show the spatially high-pass filtered fields obtained by removing variability with scales longer than  $30^\circ$  of longitude by  $10^\circ$  of latitude.*

1-Year Average Wind Stress Curl  
August 1999 – July 2000

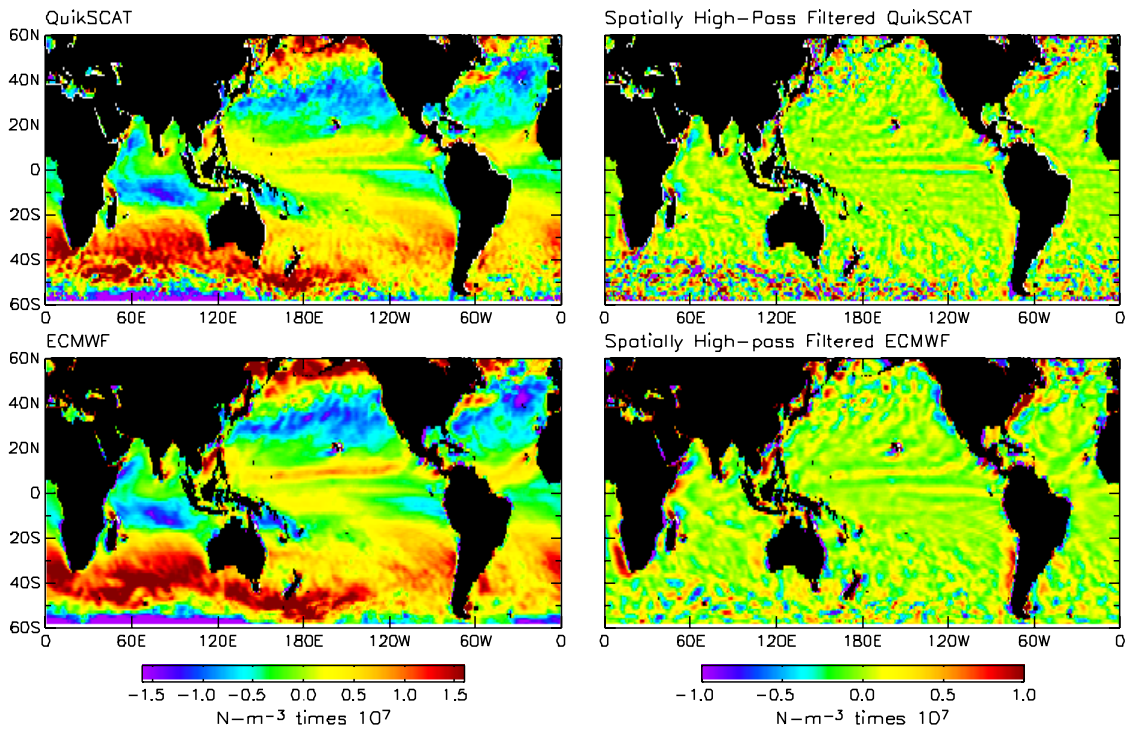


Figure 8 The same as Fig. 7, except for the wind stress curl.

SST Perturbations of Wind Stress Curl and Divergence  
30°S to 60°S, QuikSCAT vs. Reynolds, ECMWF vs. Reynolds

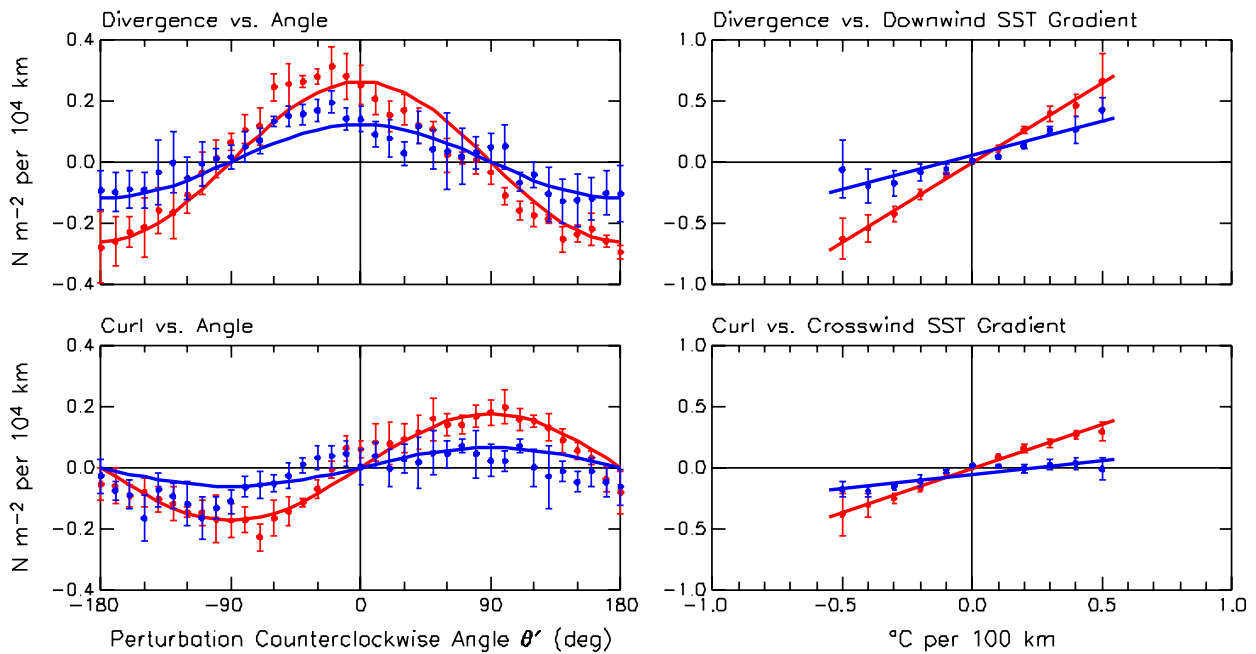


Figure 9 The same as Fig. 3, except for the latitude band 30°S to 60°S. Because TMI SST observations are not available south of 38°S, the QuikSCAT data are compared here with the Reynolds SST analyses.

Though noisier than in the eastern tropical Pacific, the short-scale variations in the wind stress divergence and curl in the Southern Ocean exhibit the same cosine and sine dependencies on the angle between the SST gradient vector and the wind direction (see the red lines in the left panels of Fig. 9). The red lines in the right panels of Fig. 9 show that the short-scale wind stress divergence and curl variations also exhibit linear

relationships to the short-scale downwind and crosswind SST gradients, respectively. The slopes of the straight-line fits are very similar to what was obtained for the eastern tropical Pacific analysis in Fig. 3, but this is probably fortuitous since SST effects on low-level winds must surely depend on the boundary layer thickness, the strength of the winds aloft, and other factors.

The global 12-month average wind stress divergence and curl fields from the ECMWF surface stress fields are shown in the lower left panels of Figs. 7 and 8. It is visually apparent that these ECMWF derivative wind stress fields are spatially smoothed representations of the wind stress divergence and curl fields from the QuikSCAT observations. This was quantified by spatially smoothing the QuikSCAT and ECMWF wind stress fields with a loess smoother with low-pass filter cutoffs of  $30^\circ$  of longitude by  $10^\circ$  of latitude, analogous to smoothing with  $18^\circ$  by  $6^\circ$  spatial averages as noted above. Binned averages of the resulting spatially low-pass filtered ECMWF wind stress divergence and curl as functions of the spatially low-pass filtered QuikSCAT derivative wind stress fields are shown in the left panels of Fig. 10. These binned scatter plots of large-scale wind stress divergence and curl fall very nearly along the line through the origin with unit slope, indicating that the large-scale wind stress field is accurately reproduced by the ECMWF model.

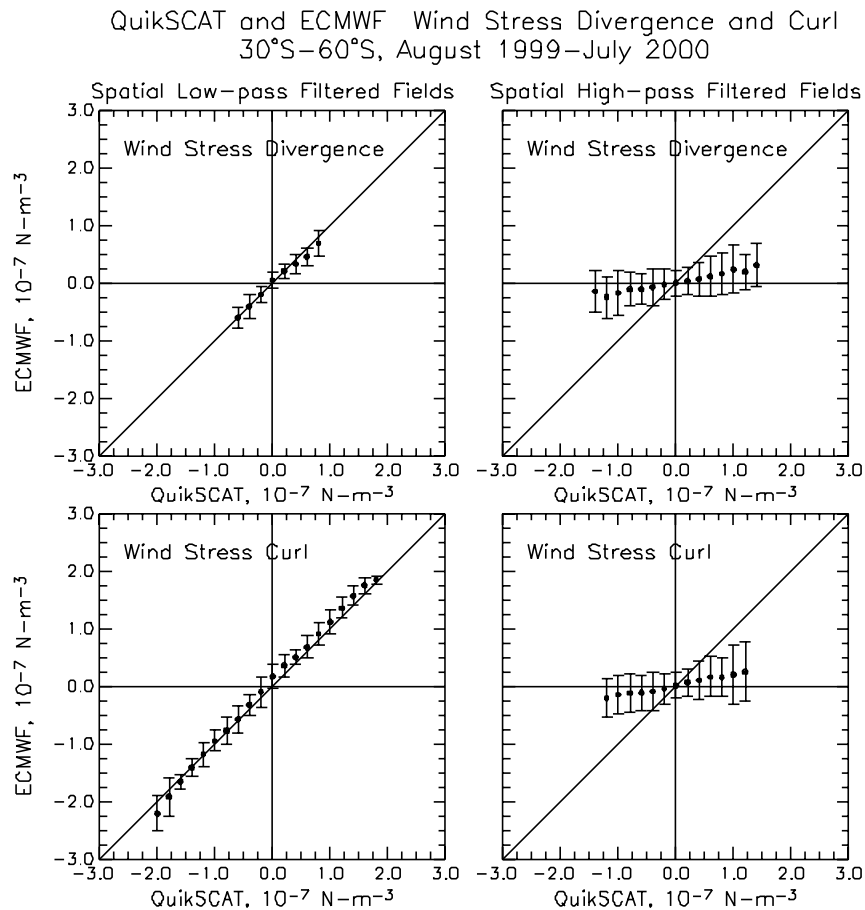


Figure 10 Binned scatter plots of ECMWF versus QuikSCAT wind stress divergence (top) and curl (bottom) on large (left) and on short (right) spatial scales. The filter cutoffs separating large and short scales are  $30^\circ$  of longitude by  $10^\circ$  of latitude. The error bars represent the standard deviations of the scatter within each bin.

The spatially high-pass filtered ECMWF derivative wind stress fields obtained by subtracting the  $30^\circ$  by  $10^\circ$  smoothed fields are shown in the lower right panels of Figs. 7 and 8. These short-scale fields exhibit patchy patterns in the same regions of patchy variability in the QuikSCAT short-scale wind stress divergence and curl fields (upper right panels of Figs. 7 and 8). Indeed, most of the individual divergence and curl anomalies with large amplitudes in the QuikSCAT fields can be identified in the ECMWF derivative wind

stress fields as well. However, the magnitudes of the short-scale perturbations are much smaller in the ECMWF fields. It is also apparent visually from the right panels of Figs. 7 and 8 that the spatial scales of these features are generally larger in the ECMWF fields. These differences are quantified in the binned scatter plots in the right panels of Fig. 10. The slopes of lines through these binned scatter plots indicate that the short-scale features in the ECMWF derivative wind stress fields are more than a factor of 5 smaller than their counterparts in the QuikSCAT derivative wind stress fields.

Although the short-scale variability of the wind stress divergence and curl fields is under-represented in the ECMWF analyses, it is seen from the blue lines in the right panels of Fig. 9 that these features are linearly related to the perturbation downwind and crosswind SST gradients in the 12-month average Reynolds SST fields, albeit with larger noise and considerably smaller amplitude than in the case of the short-scale variability in the QuikSCAT wind stress divergence and curl fields.

We conclude that the influence of SST on low-level winds observed from QuikSCAT data over the Southern Ocean is present but weak in the ECMWF winds. Since the QuikSCAT and ECMWF derivative wind stress fields are compared here with the same Reynolds SST gradient component fields, all of the differences between the QuikSCAT and ECMWF winds in Figures 7–10 are indicative of shortcomings of the ECMWF model. This appears to be due, at least in part, to resolution limitations in the ECMWF analyses; although the model grid resolution was  $0.565^\circ$  in the ECMWF wind stress fields analyzed here, it is seen from the right panels of Fig. 10 that the actual resolution of the ECMWF wind fields was evidently no better than wavelengths of  $30^\circ$  of longitude by  $10^\circ$  of latitude in the annual average considered here.

## 5. Summary and Conclusions

QuikSCAT observations of surface wind stress have revealed the existence of remarkably strong coupling between SST and low-level winds in regions of strong SST gradients throughout the world ocean. This air-sea interaction is most clearly manifested in the derivative wind stress fields (divergence and curl). Wind stress divergence and curl are linearly related to the downwind and crosswind gradients of SST, respectively. The observed SST influence on low-level winds is evidently attributable to the effects of SST-induced modifications of atmospheric stability on the vertical profile of wind in the marine boundary layer.

SST-induced perturbations of the wind stress divergence and curl fields are also evident in the ECMWF surface wind stress fields, but with much weaker intensity than in the QuikSCAT observations. From analyses in the eastern tropical Pacific (Section 3) and the Southern Ocean (Section 4), the evidence presented here suggests that inaccuracies in the surface SST boundary condition and the coarse spatial resolution of the ECMWF surface wind fields both contribute to the discrepancies between surface wind stress fields constructed from QuikSCAT observations and from the ECMWF model. Inaccuracies in atmospheric boundary layer parameterization may also be a contributing factor, but this cannot be determined from the analyses presented here.

Notwithstanding the under-representation of this air-sea interaction in the ECMWF model, the sensitivity of the ECMWF analyses to the detailed specification of the SST boundary condition (Section 3) is unequivocal evidence that SST has a significant effect on low-level winds in the ECMWF model. The response of the model winds to SST is at least qualitatively consistent, and apparently even quantitatively consistent in the eastern tropical Pacific, with the coupling between SST and winds observed in QuikSCAT data. With higher spatial resolution and a more accurate and real-time specification of the SST boundary condition, it can be anticipated that the accuracy of the ECMWF analyses of low-level winds will improve.

## References

- Chelton, D. B., and M. G. Schlax, 2003: The accuracies of smoothed sea surface height fields constructed from tandem altimeter datasets. *J. Atmos. Oceanic Technol.*, **20**, in press.
- Chelton, D. B., F. J. Wentz, C. L. Gentemann, R. A. de Szoeke and M. G. Schlax, 2000: Microwave SST observations of transequatorial tropical instability waves. *Geophys. Res. Lett.*, **27**, 1239-1242.
- Chelton, D. B., S. K. Esbensen, M. G. Schlax, N. Thum, M. H. Freilich, F. J. Wentz, C. L. Gentemann, M. J. McPhaden and P. S. Schopf, 2001: Observations of coupling between surface wind stress and sea surface temperature in the eastern tropical Pacific. *J. Climate*, **14**, 17,877-17,904.
- Hashizume, H., S.-P. Xie, W. T. Liu and K. Takeuchi, 2001: Local and remote atmospheric response to tropical instability waves: a global view from space. *J. Geophys. Res.*, **106**, 10,173-10,185.
- Hayes, S. P., M. J. McPhaden and J. M. Wallace, 1989: The influence of sea-surface temperature on surface wind in the eastern equatorial Pacific: Weekly to monthly variability. *J. Climate*, **2**, 1500-1506.
- Large, W. G., and S. Pond, 1981: Open-ocean momentum flux measurements in moderate to strong winds. *J. Phys. Oceanogr.*, **11**, 324-336.
- O'Neill, L. W., D. B. Chelton and S. K. Esbensen, 2003: Observations of SST-induced perturbations of the wind stress field over the Southern Ocean on seasonal time scales. *J. Climate*, **16**, in press.
- Reynolds, R. W., and T. M. Smith, 1994: Improved global sea surface temperature analyses using optimum interpolation. *J. Clim.*, **7**, 929-948.
- Schlax, M. G., D. B. Chelton and M. H. Freilich, 2001: Sampling errors in wind fields constructed from single and tandem scatterometer datasets. *J. Atmos. Oceanic Tech.*, **18**, 1014-1036.
- Wallace, J. M., T. P. Mitchell and C. Deser, 1989: The influence of sea surface temperature on surface wind in the eastern equatorial Pacific: Seasonal and interannual variability. *J. Climate*, **2**, 1492-1499.
- Wentz, F. J., C. Gentemann, D. Smith and D. Chelton, 2000: Satellite measurements of sea surface temperature through clouds. *Science*, **288**, 847-850.
- Xie, S.-P., M. Ishiwatari, H. Hashizume and K. Takeuchi, 1998: Coupled ocean-atmosphere waves on the equatorial front. *Geophys. Res. Lett.*, **25**, 3863-3866.